Suitability of Alloyed Steels in Highly Acidic Geothermal Environments

Amela Keserović
Helmholtz Centre Potsdam GFZ German Research Centre for Geosciences
Telegrafenberg
Potsdam, 14473
Germany

Ralph Bäßler
Federal Institute for Materials Research and Testing
Unter den Eichen 87
Berlin, 12205
Germany

Yustin Kamah
Pertamina Geothermal Energy
Jl.M.H. Thamrin No.9
Jakarta, 10340
Indonesia

ABSTRACT

This study aims to evaluate which of the materials currently available on the market could overcome the problem of corrosion and withstand highly aggressive conditions in the exploitation of geothermal resources in volcanic environments. Our investigations were triggered by the conditions on Lahendong geothermal field (North Sulawesi, Indonesia): well LHD-23 presents one of the greatest challenges due to its capacity of producing > 20 MW_e of energy from a single well and in the same time having very low pH (2 - 3) and relatively high chloride (1,500 mg/L) and sulphate (1,600 mg/L) concentration. Three different steel grades (low-alloyed steel UNS G41300, stainless steel UNS S31603 and high-alloyed stainless steel UNS N08031) were selected, and their corrosion behavior was evaluated by means of short-term electrochemical methods (potentiodynamic polarization) and long-term exposure tests (up to 6 months). The research was carried out in the laboratory under stagnant conditions in the artificial LHD-23 geothermal brine (1,500 mg/L chlorides, 1,600 mg/L sulphates, pH 2) at 100 °C (100 kPa) and 175 °C (900 kPa), simulating the conditions present at the site.

Considering the selected alloys' corrosion behavior at 100 °C, stainless steel UNS S31603 could represent an option to be used in the designed geothermal application due to its excellent performance in terms of corrosion resistance, compared to alloy UNS G41300, and lower cost, compared to alloy UNS N08031. Controversially, at 175 °C, due to the relatively low and within the acceptable limits corrosion rates of UNS G41300, low-alloyed steels could be employed as a constructional material for the geothermal power plant in stagnant highly acidic environments, as long as the wall thickness of the material vs. corrosion rate is taken into account.

Keywords: geothermal, corrosion, steel, electrochemistry, exposure tests, Lahendong

INTRODUCTION

Lahendong geothermal field, located in North Sulawesi, is one of the prospective geothermal sites in Indonesia, having a geothermal potential of 170 MW_e.[1] Currently, only 80 MW_e is being utilized and yet still enough to supply 60 % of North Sulawesi with electrical energy.[2,3] The focus of this study was on the well LHD-23, which presents one of the greatest challenges on Lahendong geothermal site due to its capacity of producing more than 20 MW_e from a single well. However, an even greater challenge represents exploiting the geothermal fluid from that well because of its very low pH (2-3) and relatively high chloride (1,500 mg/L) and sulphate (1,600 mg/L) concentration.[4,5]

During an average lifespan of approximately 30 years,[6] geothermal power plants are more than 90 % of the time in operation,[7] i.e. they are producing electrical energy. One of the major problems that could affect the stable and continuous energy production is the corrosion of constructional materials and equipment due to their interaction with an aggressive environment.[8,9] Among all of the existing electric power generation facilities, corrosion is considered to be the most severe on geothermal power plants. This can be attributed to the extreme high temperature and pressure conditions present in geothermal systems, as well as the existence of almost an entire periodic system of elements in form of corrosive salts. Therefore, geothermal fluids are found to be extremely hostile for the constructional material and equipment installed at geothermal power plants. If insufficient and inadequate measures for material selection are taken during the initial design phase of the plant, a huge risk of equipment degradation and system failure is present. This could not only lead to the reduction in the energy production, but also to the shutdown of the entire geothermal power plant.[10]

Geothermal systems consist of various constructional units required for the power plants' operation. In order to exploit the geothermal fluid from the reservoir and transfer it to the turbine in the geothermal power plant, several hundred meters of transmission pipeline is installed, along with different equipment (heat exchangers, separators, etc.) necessary for the plants' performance. The most commonly used materials for construction of these units are metallic materials, primarily steels, due to their excellent corrosion resistance in aggressive geothermal environments, appropriate mechanical properties and lower costs compared to other materials.[11-13] This study helps to evaluate which of the steel materials present at the market could overcome the problem of corrosion and withstand such an aggressive environment.

Corrosion behavior of three different grades of steel materials (low-alloyed steel UNS G41300, stainless steel UNS S31603 and high-alloyed stainless steel UNS N08031) was investigated by means of short-term electrochemical methods and long-term exposure tests. The measurements were performed in the laboratory in the artificial LHD-23 geothermal brine at 100 °C (100 kPa) and 175 °C (900 kPa) under stagnant conditions. Occasional shutdown of the plant and resulting static conditions of the corrosive brine in the pipeline and equipment could cause even more detrimental corrosion attack then during the operation conditions, due to the adsorption of the aggressive ions on the metal service, leading to the pitting corrosion initiation.[14-19]

EXPERIMENTAL PROCEDURE

The corrosion resistance of three different steel grades (low-alloyed steel UNS G41300, stainless steel UNS S31603 and high-alloyed stainless steel UNS N08031) in the artificial LHD-23 geothermal brine was evaluated by means of electrochemical methods and long-term exposure tests under stagnant conditions. The corresponding chemical composition of the investigated materials and the brine is shown in Table 1 and 2, respectively. The experiments were performed at 100 °C (100 kPa) and 175 °C (900 kPa), simulating the brine conditions present on the geothermal site Lahendong (North Sulawesi, Indonesia) in technical facilities above the ground (pipelines, separators, heat exchangers, etc.) after extraction of the geothermal fluid from the well LHD-23 and the separation of the steam and brine.

Table 1: Chemical composition of the tested materials in wt% (balance Fe)

Material	C	Si	Mn	P	S	Cr	Mo	Ni	N	Cu
UNS G41300	0.29	0.4	0.9	0.025	0.040	1.2	0.3	-	-	-
UNS S31603	0.03	1.0	2.0	0.045	0.015	18.5	2.5	13	0.11	-
UNS N08031	0.15	0.3	2.0	0.020	0.100	28.0	7.0	32	0.25	1.4

Table 2: Chemical composition of the artificial LHD-23 geothermal brine and the resulting acidity

	Cl^-	SO_4^{2-}	K^+	Na^+	pH
mg/L	1,500	1,600	200	1,000	2

Prior to each experiment, materials were wet ground with a 320 SiC sand paper, thoroughly rinsed with deionized water and degreased ultrasonically in alcohol and acetone to remove the residual impurities, according to the ASTM G1 standard.[20] In order to assure the results reproducibility, each of the experiment set was performed three times.

Due to the possibility of oxygen intrusion into the geothermal system, in the present study no method was used to remove the dissolved oxygen from the brine. However, it must be recognized that dissolved oxygen will be low at 100 °C and will also be consumed by the corrosion reactions. Reducing conditions can be assumed for the longer term experiments and to some extent for the shorter term experiments as well.

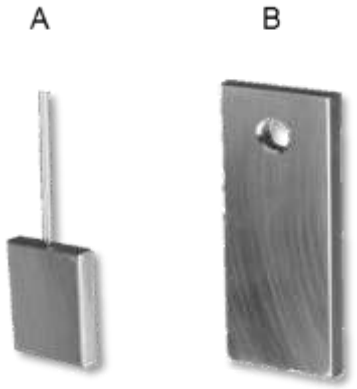

Figure 1: Material sample preparation for: A) electrochemical and B) exposure tests

Electrochemical methods

Electrochemical measurements were carried out in a standard three electrode cell, consisting of a saturated Ag/AgCl reference electrode, Ti/TiO_2 net counter electrode and a working electrode made of the investigated material. At 100 °C the experiments were performed in glass vessels equipped with water condensers. For high temperature and pressure conditions autoclaves were used, equipped with manometers for pressure control and aluminum cylinder mantles to avoid heat dissipation. External heating mantles and ceramic heating plates, together with a temperature regulator, precision ± 3 K, and Pt-100 sensor were employed to assure a constant heating during the experiments. The measurements were performed using Gamry Potentiostatic System Model Reference 600†. The obtained data were

† Trade name.

analyzed with help of Gamry Echem Analyst Software†. All of the recorded electrode potentials, mentioned in the current work, are referred to a standard Ag/AgCl reference electrode potential.

In the current study the system stabilized ($\Delta E_{oc} \leq 5$ mV/10 min[21]) after several hours of immersion. In order to obtain a comparable corrosion behavior of the selected materials, the electrochemical methods were conducted after 20 h of immersion. To study the corrosion behavior of low-alloyed steel UNS G41300 Tafel extrapolation method was performed ± 200 mV vs. the corresponding open circuit potential, E_{oc}, with a 0.2 mV/s sweep rate. The corrosion rate was calculated from the corrosion current density, j_{corr}, obtained from the intersection of the corrosion potential line and Tafel branch that showed the linearity over at least one decade of j_{corr}, according to the equation:[22]

$$CR = \frac{j_{corr} \cdot EW}{F \cdot \rho} \cdot 3.15 \cdot 10^5 \quad (1)$$

where CR is corrosion rate (mm/y), j_{corr} corrosion current density (mA/cm²), EW material equivalent mass (g/mol), F Faraday constant (96,500 A s/mol) and ρ material density (g/cm³).

Susceptibility of the alloys UNS S31603 and UNS N08031 to pitting corrosion was studied by means of cyclic polarization method. The potential scan was introduced at -200 mV relative to E_{oc} and proceeded in the anodic direction with 0.2 mV/s linear sweep rate. As soon as E = 1.2 V vs. E_{oc} or j_{corr} = 2 mA/cm² was reached, the scan was reversed in the cathodic direction, back to -200 mV vs E_{oc}. Pitting potential, E_{pit}, was determined when the current on the forward scan rapidly increases, and repassivation potential, E_{rep}, when the hysteresis on the backward scan closes the loop.

Exposure tests

The investigated materials were prepared according to the ASTM G1 standard,[20] weighed on an analytical laboratory scale (precision 10^{-4} g), and completely immersed vertically in the artificial LHD-23 geothermal brine for 1, 3 and 6 months at 100 °C (100 kPa) and 175 °C (900 kPa). In order to prevent interactions between different types of materials and their corrosion products all materials were tested separately. After exposure, the corrosion products were firstly removed mechanically, using a paper towel and a nonmetallic bristle brush. Afterwards, chemical cleaning was followed in an ultrasonic bath, immersing the coupons in the solution specifically designed to remove the corrosion products with minimal dissolution of the base metal. For this purpose an aqueous solution of 250 mL/L HCl (conc.) containing 3.5 g hexamethylenetetramine was used for pickling the surface of UNS G41300, and a mixture of 100 mL/L HNO_3 and 20 mL/L HF (4 wt%) for cleaning UNS S31603 and UNS N08031.[20,23] The coupons were subsequently weighed on the same analytical scale as prior to the exposure. The corrosion rate was determined according to the equation:[20]

$$CR = \frac{m_2 - m_1}{A \cdot t \cdot \rho} \cdot 10^3 \quad (2)$$

where CR is corrosion rate (mm/y), m_1 and m_2 coupon masses (g) before and after the exposure and removal of corrosion products, A surface area of the exposed coupon (mm²), t time of exposure (y), and ρ material density (g/cm³). Furthermore, the surface of the coupons was visually analyzed using an optical microscope with a 2000-fold magnification to determine the type of corrosion attack and to characterize the pits in case of pitting corrosion occurrence.

At 100 °C the tests were performed in glass vessels equipped with water condensers to avoid water evaporation. For high temperature and pressure conditions autoclaves were used. During the exposure, the equipment was put in a climate chamber that provided the needed heat and uniform temperature distribution.

RESULTS

Low-alloyed steel UNS G41300

Electrochemical tests

Open circuit potentials, E_{oc} (i.e. E_{corr}), of low-alloyed steel UNS G41300 showed rather negative values in the artificial LHD-23 geothermal brine (Figure 2), suggesting high surface activity. Increasing the temperature from 100 °C to 175 °C a slight ennoblement of the potentials was observed, which could be attributed to the formation of a corrosion layer with somewhat protective characteristics.

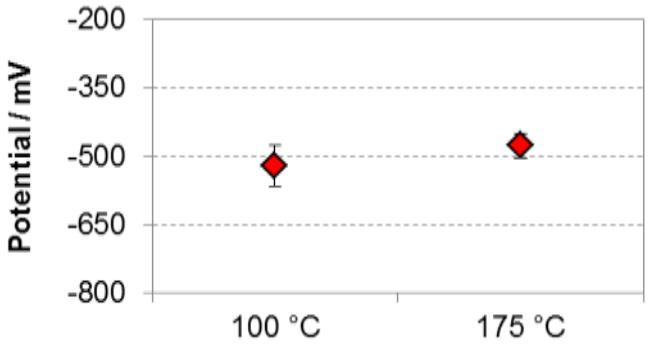

Figure 2: Temperature influence on open circuit potentials of low-alloyed steel UNS G41300 in the artificial geothermal LHD-23 geothermal brine

In the current study Tafel extrapolation method was employed to evaluate and predict the corrosion rates of UNS G41300 at different temperatures. Considering the conditions in which the polarization curves were generated (pH 2, negative open circuit potentials, aerated conditions) proposed mechanisms for the reactions occurring on the electrodes are the following:

- cathode:

$$2H^+ \rightarrow H_2 + 2e^- \quad (3)$$

- anode:

$$Fe \rightarrow Fe^{2+} + 2e^- \quad (4)$$

$$Fe^{2+} \rightarrow Fe^{3+} + e^- \quad (5)$$

Increasing the temperature the polarization curves shifted toward positive potentials and higher corrosion current densities (Figure 3), pointing out to the higher electrode dissolution rates at 175 °C. From the intersection of the extrapolated linear cathodic and anodic branches at zero overpotential, corrosion current was determined. Subsequently, according to Equation (1), corrosion rate calculated (Table 3).

An increase of the rate of more than three times with the temperature elevation was, presumably, overestimated due to the imprecise Tafel slope determination, caused by the non-linearity of the corresponding anodic and cathodic regions. This could be linked to the accumulation of ferric compounds and hydrogen bubbles on the electrode surface, thereby impairing the diffusion of oxidants and causing the concentration effect. Eventually, it could result in the corrosion rate reduction with further exposure time of the metal in the corrosive environment.

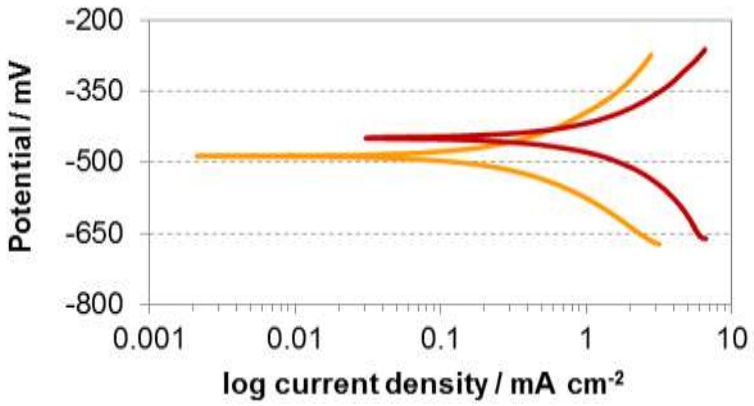

Figure 3: Typical anodic and cathodic polarization curves for low-alloyed steel UNS G41300 in artificial LHD-23 geothermal brine at: (—) 100 °C and (—) 175 °C

Table 3: Electrochemical variables determined with Tafel extrapolation method

T / °C	B_a / mV dec^{-1}	B_c / mV dec^{-1}	E_{corr} / mV	j_{corr} / mA cm^{-2}	CR / mm y^{-1}
100	212.9	206.8	-485.9	0.3805	4.41
175	256.7	263.9	-449.4	1.3470	15.62

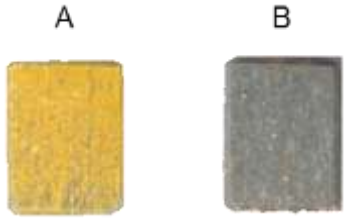

Figure 4: Low-alloyed steel UNS G41300 electrode appearance after dynamic polarization in the artificial LHD-23 geothermal brine at: A) 100 °C and B) 175 °C

Exposure tests

Low-alloyed steel UNS G41300 experienced uniform corrosion. Corrosion rates, calculated from the coupons weight loss according to Equation (2), are shown in Figure 5. Rather high metal dissolution rates, above the acceptable limits (≥ 1 mm/y) are observed at 100 °C. Moreover, they tended to linearly increase with further exposure time. Such behavior could be attributed to the high solution acidity, causing dissolution of corrosion products formed on the surface and thus, direct contact between the bare metal surface and corrosive environment. Increasing the temperature to 175 °C corrosion rates were within the acceptable limits and they tended to decrease with subsequent exposure. Such behavior suggests the formation of a corrosion layer, presumably ferric oxide, with somewhat protective characteristics.

The main reason why the corrosion rates at 100 °C are up to one order of magnitude higher than at 175 °C could be linked to the oxygen content in the solution. At 100 °C only traces of oxygen are present in the solution due to its decreased solubility, hindering the formation of more stable ferric compounds. However, at 175 °C the pressure of the system increases, as well as the oxygen partial pressure. Therefore, the concentration of oxygen in the solution was higher, enabling the formation of stable ferric compounds on the metal surface and thus, reduction of the metal dissolution rates.

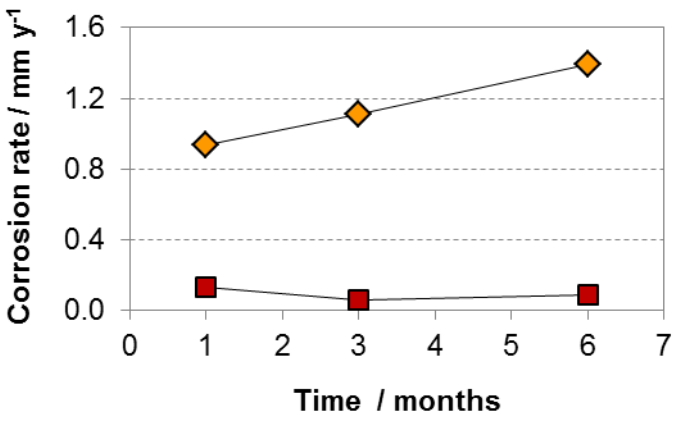

Figure 5: Corrosion rates of UNS G41300 after exposure tests in the artificial LHD-23 geothermal brine at: (◆) 100 °C and (■) 175 °C

Comparing the results obtained with short-term electrochemical methods (Tafel extrapolation) and long-term exposure tests, significant discrepancy was observed (Table 3, Figure 5). This is explained with the fact that an adherent corrosion product layer forms on the metal surface with time, decreasing the corrosion rate. Since Tafel extrapolation method is a short-time test and it was performed within the first two days of the material immersion in the solution, the layer was not as evolved as during the subsequent 6 months of exposure, resulting in higher corrosion rates compared to the weight loss tests.

Stainless steel UNS S31603

Electrochemical tests

Increasing the temperature open circuit potentials, E_{oc}, of stainless steel UNS S31603 shifted in the anodic direction (Figure 6) implying to an ennoblement of the electrode surface, presumably due to the formation of more protective (e.g. thicker, more compact) passive layer. However, interpretation of E_{oc} can sometimes be misleading. An increase of the E_{oc} could lead also to the reduction of the passive range and earlier onset of pitting corrosion. Therefore, cyclic polarization was performed in order to establish the passivity range of the alloy and determine the critical potentials.

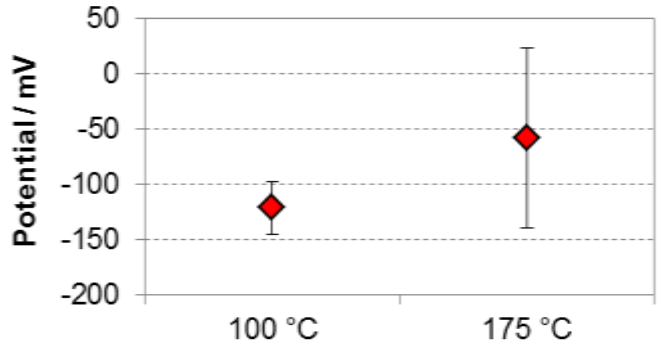

Figure 6: Temperature influence on open circuit potentials of stainless steel UNS S31603 in the artificial geothermal LHD-23 geothermal brine

At 100 °C electrode surface of UNS S31603 was passive over an extensive potential range (Figure 6, Table 4). Relatively noble pitting potential, E_{pit}, suggests excellent resistance to pitting corrosion. However, once the pitting onset, a wide negative hysteresis was present, visible on the backward scan. Such observation implies to a significant surface disruption, i.e. pit initiation and propagation, due to the

anodic polarization, as can be seen from the numerous pits formed on the surface shown in Figure 8: A. Accordingly, surface repassivation of the attacked sites was delayed, as noted from the rather high distance between repassivation and pitting potentials. Increasing the temperature to 175 °C the alloy exhibited active-passive behavior in the applied potential range (spike at ca. -250 mV in Figure 7), more negative than the corresponding E_{oc}. Furthermore, E_{pit} shifted in the active direction. All of these facts imply to a reduction in the passivity range of the electrode surface and to an earlier onset of pitting corrosion. On the backward scan the current density ceased rather quickly to lower values, causing a narrower negative hysteresis. However, the complete repassivation of the electrode surface was achieved at the potentials more active than the corresponding E_{oc}, indicating a poor repassivation capability of the attacked sites and a possibility of metastable pitting to occur in the normal stagnant service conditions. Surface analysis of the electrodes after cyclic polarization revealed similar number of pits formed on the surface as at 100 °C, only larger and deeper (Figure 8: B). Such observations could be attributed to the higher diffusion rates of chlorides and sulphates present in the solution that are responsible for pitting corrosion.

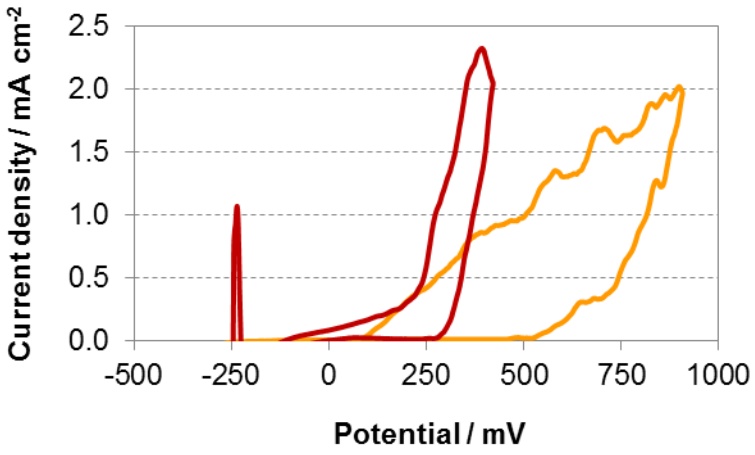

Figure 7: Temperature influence on typical anodic and cathodic polarization curves for stainless steel UNS S31603 in artificial LHD-23 geothermal brine at: (—) 100 °C and (—) 175 °C

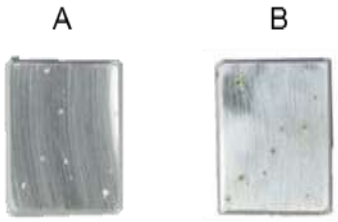

Figure 8: Stainless steel UNS S31603 electrode appearance after cyclic polarization in the artificial LHD-23 geothermal brine at: A) 100 °C and B) 175 °C

Table 4: Electrochemical variables determined with cyclic polarization method

T / °C	E_{oc} / mV	E_{rep} / mV	E_{pit} / mV
100	-121.3	66.6	518.9
175	-58.5	-114.0	304.7

Exposure tests

Stainless steel UNS S31603 exhibited extremely low mass loss at 100 °C (< 0.0001 g) during the whole exposure time. Accordingly, the corrosion rate was considered to be < 0.06 µm/y. Such finding proves excellent resistance of the alloy to uniform corrosion. Furthermore, no signs of pitting corrosion are observed on the coupon surface, indicating resistance to pitting corrosion as well. However, light deposits are found on the surface, which could eventually, with further exposure time, result in a passive film breakdown (Figure 10: A).

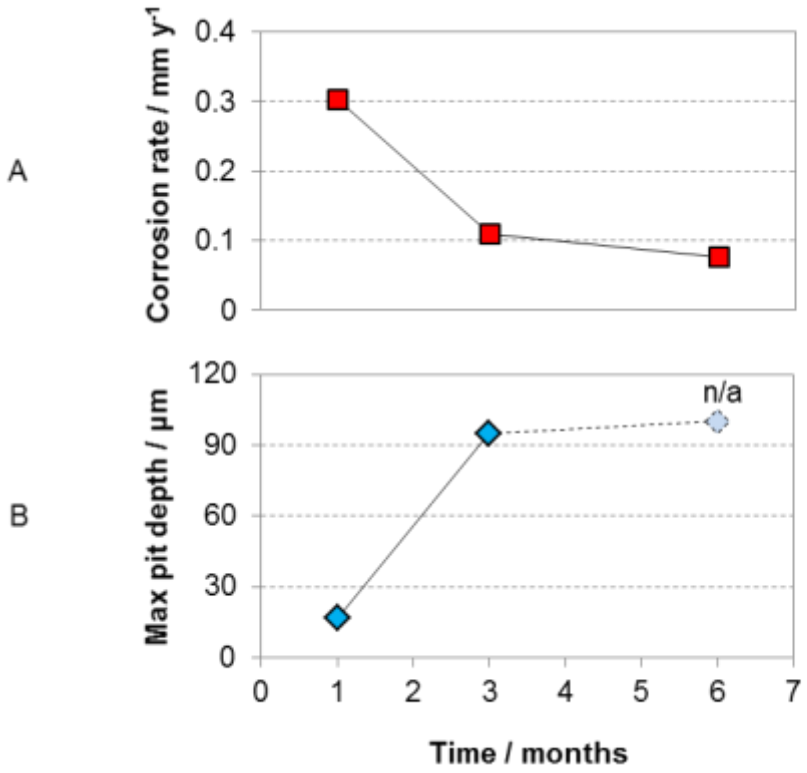

Figure 9: A) Corrosion rate and B) maximum pit depth of UNS S31603 determined after exposure in the artificial LHD-23 geothermal brine at 175 °C

At 175 °C a uniform passive film disruption was clearly evident (Figure 10: B), suggesting solubility of the passive layer due to the extremely acidic conditions. The calculated corrosion rate reached 0.3 mm/y during the first month of exposure (Figure 9: A). With the subsequent exposure time the metal dissolution rate was reduced, suggesting the formation of an adherent, tenacious corrosion layer. Visual inspection of the coupons implied to the formation of different ferric oxides on the surface. A clear evidence of pitting corrosion was observed after 1 and 3 months, showing pit propagation with the exposure time, indicated by the increase of the pit depth (Figure 9: B). After 6 months of exposure pitting corrosion was present as well, but due to the severe uniform corrosion and very dense pits formed on the surface, it was hard to distinguish uniform metal dissolution from the localized attack, implying to an extremely intensive corrosion.

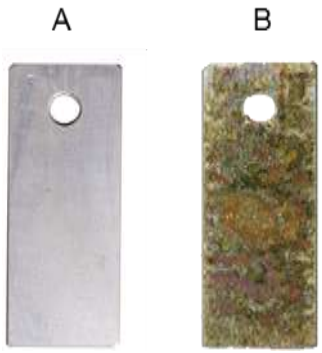

Figure 10: UNS S31603 coupons appearance after 6 months of exposure in the artificial LHD-23 geothermal brine at: A) 100 °C and B) 175 °C

High-alloyed stainless steel UNS N08031

Electrochemical tests

Open circuit potentials of high-alloyed stainless steel UNS N08031 stabilized at negative values after 20 h of immersion in the artificial LHD-23 geothermal brine (Figure 11). At higher temperature E_{oc} shifted in the anodic direction, indicating surface ennoblement, presumably due to the formation of a passive layer with better protective characteristics.

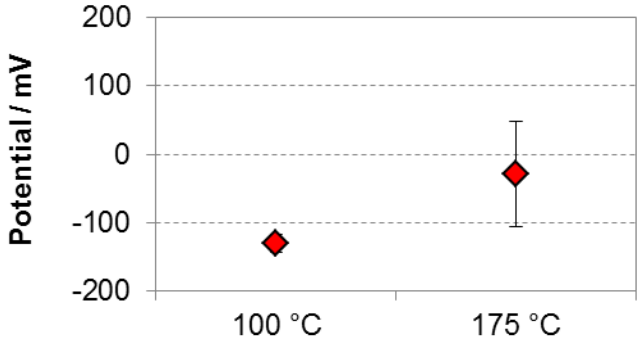

Figure 11: Temperature influence on open circuit potentials of high-alloyed stainless steel UNS N08031 in the artificial geothermal LHD-23 geothermal brine

At 100 °C a large passivity range was observed, extending over more than 900 mV (Figure 12, Table 5). Such behavior points out to the excellent pitting corrosion resistance of the alloy in the investigated conditions. Furthermore, on the backward scan the current density ceased quickly to the initial values, showing an outstanding repassivation capability of the surface. In contribution to this speaks also the absence of a hysteresis, indicating also very small surface disruption and quick repassivation of the attacked sites. Surface analysis of the electrodes after the cyclic polarization tests using an optical microscope revealed extremely small and shallow pits (Figure 13: A), corroborating the conclusions based on the visual observation of the curves.

Increasing the temperature to 175 °C E_{pit} shifted to more active values, showing an increased susceptibility to pitting corrosion. The passivity range was still rather large, but the metastable area increased due to a substantial reduction of E_{rep} in the cathodic direction. Accordingly, large negative hysteresis was present on the backward scan, indicating significant surface disruption. This was supported by the surface analysis of the electrode (Figure 13: B) that showed a small amount of pits present on the surface, but relatively large and deep. However, since the E_{rep} was still more positive

than the corresponding E_{oc}, it is considered that the alloy would experience stable passivity during the normal stagnant service conditions and it would have a good repassivation capability.

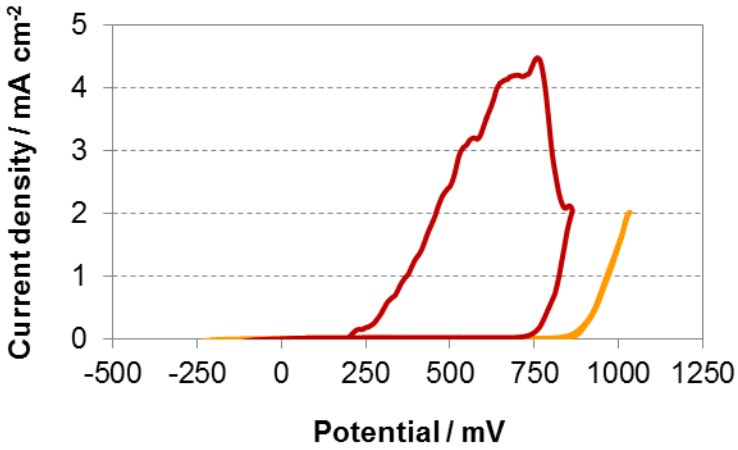

Figure 12: Temperature influence on typical anodic and cathodic polarization curves for high-alloyed stainless steel UNS N08031 in artificial LHD-23 geothermal brine at: (—) 100 °C and (—) 175 °C

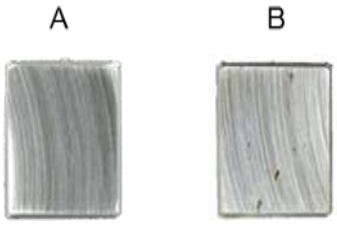

Figure 13: High-alloyed stainless steel UNS N08031 electrode appearance after cyclic polarization in the artificial LHD-23 geothermal brine at: A) 100 °C and B) 175 °C

Table 5: Electrochemical variables determined with cyclic polarization method

T / °C	E_{oc} / mV	E_{rep} / mV	E_{pit} / mV
100	-130.4	809.9	869.7
175	-29.0	191.4	751.4

Exposure tests

Weight loss method revealed extremely low mass loss of alloy UNS N08031 during the exposure time at 100 °C (< 0.0001 g). Accordingly, the calculated corrosion rates are < 0.06 µm/y. Furthermore, no pits were observed on the coupons surface even after 6 months of exposure. They retained the metal glow exhibiting an excellent resistance to uniform and pitting corrosion in the investigated highly acidic conditions at 100 °C during 6 months of exposure (Figure 15: A).

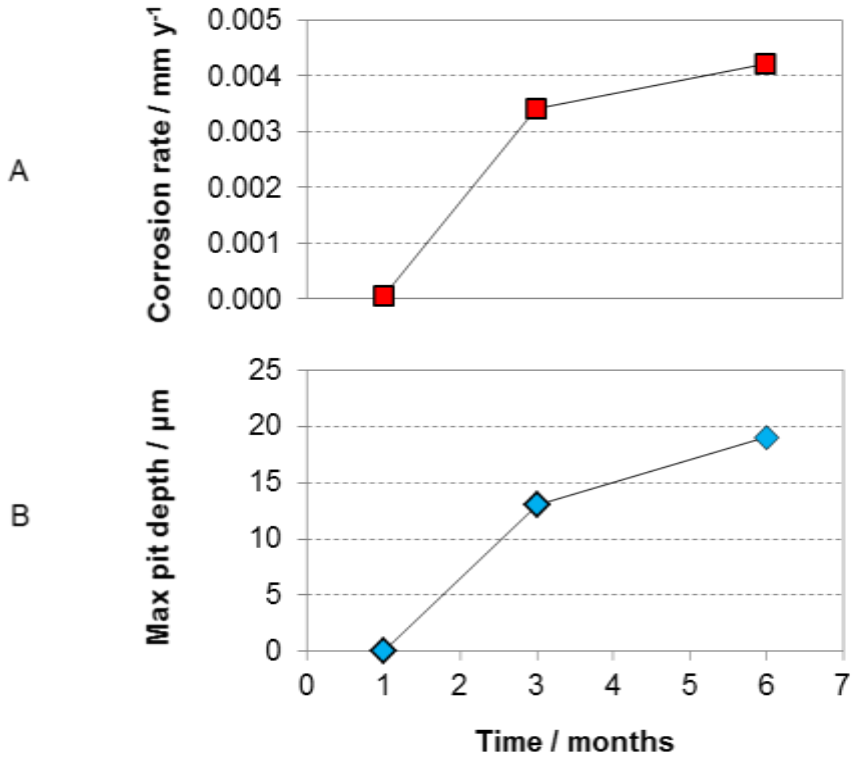

Figure 14: A) Corrosion rate and B) maximum pit depth of UNS S31603 determined after exposure in the artificial LHD-23 geothermal brine at 175 °C

Similar behavior was noticeable at 175 °C, but only after the first month of exposure. After the third month measurable corrosion rates were obtained, that increased with the subsequent exposure time (Figure 14: A), implying to the dissolution of the passive layer and its impaired capability of self-repair. Closer inspection of the material surface revealed the presence of numerous pits. Increasing the exposure time, the pits depth increased as well (Figure 14: B). Considering a greater increase in pit depth than the corrosion rate with time, one can conclude that the weight loss method is not an adequate method in determining the rate of localized corrosion, as stated in numerous literatures. On contrary, it can provide misleading results, which could cause a failure of the system.

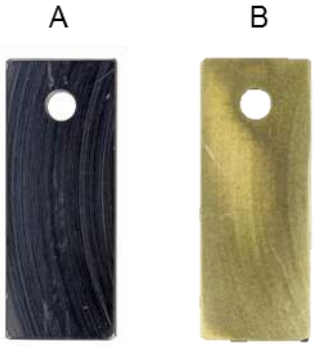

Figure 15: UNS N08031 coupons appearance after 6 months of exposure in the artificial LHD-23 geothermal brine at: A) 100 °C and B) 175 °C

CONCLUSIONS

Corrosion behavior of three different steel grades was evaluated in the highly acidic LHD-23 geothermal brine at 100 °C (100 kPa) and 175 °C (900 kPa) by means of short-term electrochemical methods and long-term exposure tests under stagnant conditions. The following are major conclusions obtained from the study:

1. Low-alloyed steel UNS G41300 exhibited corrosion rates above acceptable limits at 100 °C in stagnant conditions, which increased with exposure time. At 175 °C the dissolution rates were significantly lowered (up to one order of magnitude) and they tended to decrease. Short-term electrochemical methods showed overestimated corrosion rates.
2. Stainless steel UNS S31603 exhibited excellent resistance to uniform and pitting corrosion during the short-term electrochemical tests. The repassivation capability was significantly reduced at 175 °C. Exposure tests revealed stable passive layer formation at 100 °C during the 6 months of exposure, with no signs of any corrosion attack. At 175 °C uniform and pitting corrosion took place on the metal surface.
3. High-alloyed stainless steel UNS N08031 showed remarkable resistance to uniform and pitting corrosion, and a good repassivation capability even at 175 °C. During the 6 months of exposure at 100 °C no signs of any corrosion attack were visible on the surface. With the temperature increase to 175 °C pits initiated and propagated with time, indicating the alloy's susceptibility to pitting corrosion.

Considering the selected alloys' corrosion behavior at 100 °C, stainless steel UNS S31603 could represent an option to be used in the designed geothermal application due to its excellent performance in terms of corrosion resistance, compared to alloy UNS G41300, and lower cost, compared to alloy UNS N08031. Controversially, at 175 °C, due to the relatively low and within the acceptable limits corrosion rates of UNS G41300, low-alloyed steels could be employed as constructional materials for the geothermal power plant in stagnant highly acidic environments, as long as the wall thickness of the material vs. corrosion rate is taken into account.

However, additional tests, such as stress corrosion cracking and crevice corrosion, need to be performed prior to making any final conclusions on the materials suitability in the investigated conditions. Verification in the real brine is always advisable for proving the laboratory investigations reliability. The authors are currently working on testing the selected materials susceptibility to the formerly mentioned types of localized corrosion. The results will be reported in the future publications.

ACKNOWLEDGEMENTS

The authors would like to acknowledge the German Federal Ministry of Education and Research for its financial support within the project *Sustainability concepts for exploitation of geothermal reservoirs in Indonesia – capacity building and methodologies for site deployment* under grant 03G0753A, BMBF. The support of the Pertamina Geothermal Energy team in Jakarta, as well as at Lahendong site, including the access to the data and the field is highly appreciated. The authors thank Pertamina Geothermal Energy for the permission to publish this paper.

REFERENCES

1. B. L. Maluegha, "Calculation of Gross Electrical Power from the Production Wells in Lahendong Geothermal Field in North Sulawesi, Indonesia" (Master Thesis, Murdoch University, 2010).
2. M. Jaya, "Notes & Summary: Indonesia Visit to PGE, BPPT, ITB, Wika Jabar Power, Star Energy (Wayang Windhu), Batan, Dinas ESDM (Internal Report)," GFZ, Potsdam, Germany, 2011.
3. H. Koestono, "Lahendong Geothermal Field, Indonesia: Geothermal model Based on Wells LHD-23 and LHD-28," Geothermal Training Programme, no. 3, 2010.

4. M. Brehme et al., "Hydrochemical Patterns in a Structurally Controlled Geothermal System," *Mineralogical Magazine* 2013.
5. M. Brehme et al., "A Hydrotectonic Model of a Geothermal Reservoir Supported by Hydrogeology," *Geothermics* (in revision).
6. C. N. Hance, "Factors Affecting Costs of Geothermal Power Development," Geothermal Energy Association, 2005.
7. A. Kagel, D. Bates, K. Gawell, "A Guide to Geothermal Energy and the Environment," Geothermal Energy Association, 2007.
8. E. Huenges, P. Ledru, *Geothermal Energy Systems: Exploration, Development, and Utilization* (John Wiley & Sons, 2010).
9. M. Stapleton, "Scaling and Corrosion in Geothermal Operation," PowerChem Technology, 2002.
10. F. A. Magaly et al., "The Neutralization of Acid Fluids: An Alternative of Commercial Exploitation Wells on Los Humeros Geothermal Field," World Geothermal Congress, paper no. 2741 (Bali, Indonesia, 2010).
11. M. F. Conover, P. Ellis, "Materials Selection Guidelines for Geothermal Energy Utilization Systems," U.S. Deptartment of Energy, Division of Geothermal Energy, DOE/RA/27026-1, 1981.
12. J. P. Carter, S. D. Cramer, "Materials of Construction for High-Salinity Geothermal Brines," U.S. Bureau of Mines, RI 9402, 1992.
13. K. D. Rafferty, "Piping," *Geo-Heat Center* 19, 1 (1998).
14. L. Xu et al., "Corrosion of Cr Bearing Low Alloy Pipeline Steel in CO2 Environment at Static and Flowing Conditions," *Applied Surface Science* 270 (2013).
15. M. Kondo et al., "Corrosion of Reduced Activation Ferritic Martensitic Steel Jlf-1 in Purified Flinak at Static and Flowing Conditions," *Fusion Engineering and Design* 85, no. 7–9 (2010).
16. X. Jiang, Y. G. Zheng, W. Ke, "Effect of Flow Velocity and Entrained Sand on Inhibition Performances of Two Inhibitors for CO2 Corrosion of N80 Steel in 3% NaCl solution," *Corrosion Science* 47, no. 11 (2005).
17. R. Galvan-Martinez et al., "Characterization of the Corrosion Kinetic of X52 Steel in Seawater with Biocides," MRS Proceedings (2009).
18. F. B. Waanders, S. W. Vorster, G. J. Olivier, "Corrosion Products Formed on Mild Steel Samples Submerged in Various Aqueous Solutions," Hyperfine Interactions 139, no. 1-4 (2002).
19. I. Stănăşel et. al, "Control of Corrosion and Scaling in Selected Geothermal Wells from Romania," World Geothermal Congress 2010, paper no. 2727 (Bali, Indonesia, 2010).
20. ASTM G 1, "Standard Practice for Preparing, Cleaning, and Evaluating Corrosion Test Specimens," (West Conshohocken, PA: ASTM, 2011).
21. R. G. Kelly et al., *Electrochemical Techniques in Corrosion Science and Engineering*, 1st ed. (CRC Press, 2002).
22. ASTM G 102 (latest revision), "Standard Practice for Calculation of Corrosion Rates and Related Information from Electrochemical Measurements," (West Conshohocken, PA: ASTM, 2010).
23. R. D. Angal, *Principles and Prevention of Corrosion* (Narosa Publishing House, 2010).